Electronic Supplementary Material (ESI) for Chemical Science.

Supporting Information for:

A metal-organic framework/polymer derived catalyst containing single-atom nickel species for electrocatalysis†

Shuliang Yang‡,[a] Jie Zhang‡,[a,b] Li Peng,[c] Mehrdad Asgari,[a] Dragos Stoian,[a] Ilia Kochetygov,[a] Wen Luo,*[a,b] Emad Oveisi,[d] Olga Trukhina,[a] Adam H. Clark,[e] Daniel T. Sun,[a] and Wendy L. Queen*[a]

[a] *Institute of Chemical Sciences and Engineering, École Polytechnique Fédérale de Lausanne (EPFL), EPFL-ISIC-Valais, Sion, 1950, Switzerland*
E-mail: wendy.queen@epfl.ch

[b] *Empa Materials Science & Technology, CH-8600 Dübendorf, Switzerland*
E-mail: wen.luo@epfl.ch

[c] *College of Chemistry and Chemical Engineering, Xiamen University, Xiamen, 361005, China*

[d] *Interdiciplinary Center for Electron Microscopy, École Polytechnique Fédérale de Lausanne (EPFL), CH-1015 Lausanne, Switzerland.*

[e] *Paul Scherrer Institute, Forschungsstrasse 111, 5232 Villigen, Switzerland*

‡These authors have contributed equally to this study.

Experimental Section

Materials: Naphthalene-1,4,5,8-tetracarboxylic dianhydride (>97.0%) was supplied by TCI. 5-Amino-2-hydroxybenzoic acid was provided by Merck. Dopamine hydrochloride (99%) was purchased from Sigma-Aldrich. Nickel(II) nitrate hexahydrate (99.9% Ni) was bought from ABCR. Free-base dopamine and naphthalene diimide salicylic acid (H_4NDISA) were synthesized according to our previous reports.[1, 2]

MOF synthesis:

Synthesis of Ni_2(NDISA): Ni_2(NDISA) MOF was synthesized following previous reports but in large scale synthesis.[2, 3] Typically, 520 mg of $Ni(NO_3)_2.6H_2O$ and 275 mg of naphthalene diimide salicylic acid were ultrasonicated for 25 min in the solution of 37.5 mL of *N*,*N*-dimethyl formaldehyde (DMF), 2.5 mL of water and 2.5 mL of ethanol. The jar was tightly capped and placed in oven for 24 h at 120 °C to yield earthy yellow powder. After cooling down to room temperature and decanting the mother liquor, the product was rinsed with DMF and methanol and dried under vacuum for 8 h. To remove the residual ligands and salts inside Ni_2(NDISA), the powder was soxhleted with methanol overnight and the left Ni_2(NDISA) was dried under vacuum for further use.

Synthesis of Ni_2(NDISA)-PDA: Generally, 300 mg of Ni_2(NDISA) MOF was dispersed in 42 mL of methanol under ultrasonic, then 155 mg of free-base dopamine dissolved in 15 mL methanol was added into the Ni_2(NDISA) suspension dropwise. After stirring at room temperature for 12 h, the black product was collected by centrifugation, washed with methanol and dried under vacuum.

Synthesis of Ni/NC: 200 mg of Ni_2(NDISA) MOF in a ceramic boat was put in tubing furnace, after flushing with argon for half hour to remove the air inside, the Ni_2(NDISA) was pyrolyzed at 1000 ^{o}C for 2 h with temperature ramp of 10 ^{o}C/min. After cooling down, the black powder was etched with 3 mol/L HCl aqueous solution for 12 h. The left material was filtered and washed with 0.5 mol/L $KHCO_3$ aqueous solution and water few times. The recovered material was dried under vacuum overnight.

Synthesis of Ni/NC-D: 400 mg of Ni_2(NDISA)-PDA in a ceramic boat was put in tubing furnace, after flushing with argon for half hour to remove the air inside, the Ni_2(NDISA)-PDA was pyrolyzed at 1000 ^{o}C for 2 h with temperature ramp of 10 ^{o}C/min. After cooling down, the black powder was etched with 3 mol/L HCl aqueous solution for 12 h. The left material was filtered and washed with 0.5 mol/L $KHCO_3$ aqueous solution and water few times. The recovered material was dried under vacuum overnight for further use.

Synthesis of Ni/N-CNTs: 8.0 g of melamine and 150 mg of Ni_2(NDISA)-PDA were placed in separate boats. Then the melamine containing boat was placed upstream from the boat containing Ni_2(NDISA)-PDA in the tube furnace. This was done so that the reducing gases produced during melamine decomposition (NH_3 and H_2) would be introduced to the MOF composite facilitating the formation of CNTs and also provide an extra source of nitrogen. After flushing the tube furnace with argon for a half hour to remove the air inside, the Ni_2(NDISA)-PDA and melamine were subsequently pyrolyzed at 1000 ^oC for 2 h with temperature ramp of 10 ^oC/min under a dynamic argon flow. After cooling down, the black powder was etched with 3 mol/L HCl aqueous solution for 12 h. The left material was filtered and washed with 0.5 mol/L $KHCO_3$ aqueous solution and water few times. The recovered material was dried under vacuum overnight for further characterizations.

Characterizations: X-ray diffraction (XRD) patterns were performed on a Bruker D8 diffractometer with Cu Kα radiation (λ= 1.5418 Å) at 40 kV and 40 mA. The morphology and microstructures of the samples were characterized by scanning electron microscopy (FEI Teneo SEM) and transmission electron microscopy (FEI Tecnai G2 Spirit Twin). Scanning electron microscopy (SEM) analysis was performed on a Thermo-Scientific Teneo at an accelerating voltage of 1.00 kV and using a beam current of 100 pA. SEM images were acquired with an in-column (Trinity) detector. Energy dispersive X-ray (EDX) spectra were acquired using an X-Flash silicon drift detector from Bruker at 20 kV with a beam current of 1.6 nA. Conventional bright-field transmission electron microscopy (BF-TEM) images were acquired with a Thermo-Scientific Tecnai G2 Spirit Twin at an accelerating voltage of 120 kV. High-angle annular dark-field (HAADF) images and EDXS elemental maps were acquired with a Cs-corrected Thermo-Scientific Titan Themis 60-300 in scanning TEM (STEM) mode at an accelerating voltage of 200 kV. This microscope is equipped with a high brightness X-FEG gun and silicon drift Super-X EDX detectors. XPS measurement was performed using a Physical Instruments AG PHI VersaProbe II scanning XPS microprobe. Analysis was performed using a monochromatic Al Kα X-ray source of 24.8 W power with a beam size of 100 μm. Nitrogen adsorption-desorption isotherms were obtained on a BELSORP-max instrument at 77 K. The surface area of the materials was measured by the Brunauer-Emmett-

Teller (BET) method. The IR data was obtained on PerkinElmer Frontier Spectrometer in ATR mode. In-situ IR data were collected in transmission mode on a self-supported wafer of sample using a custom-built infrared cell at 150 K. The X-ray absorption spectroscopy (XAS) measurements were performed at the Ni K edge (8333 eV) using the QEXAFS setup of the SuperXAS beamline (SLS, Villigen).[4] The storage ring operated at 2.4 GeV in top-up mode with a ring current of 400 mA. The polychromatic X-ray beam resulting from a 2.9 T bending magnet was collimated by a silicon coated collimating mirror (which also served to reduce higher-order harmonics) and monochromatised by a Si (111) channel-cut monochromator. A Rh coated toroidal focusing mirror was used with a focal spot size on the sample position of 500 um x 200 um (H x V). Transmission geometry measurements were performed with 1.5 bar N_2 filling of the 15 cm ionization chambers and with a monochromator oscillation frequency of 1 Hz. Data extraction and processing was performed with ProQEXAFS[5] using Butterworth filtering for high frequency noise suppression and interpolation onto a defined energy grid to reduce the data point density for further analysis. The data were then subsequently averaged over a 600 s total acquisition per sample.

Details on the EXAFS analysis: Athena and Artemis software (i.e. Demeter package) were used for the data analysis (background subtraction, normalization, etc.) of the Ni K-edge XAS data and EXAFS fittings, respectively.[6] The theoretical model used for the EXAFS fitting was generated from metallic nickel foil and nickel (II) phthalocyanine standards. The amplitude reduction factor, S_0^2, was determined for the Ni metal reference and transferred to all the other samples in order to reduce the number of refined parameters, while the coordination number (C.N.) and interatomic distances ($R_{final} = R_0 + \Delta R$, R_{final} is the refined path length, R_0 is the initial path length and ΔR is the change in path length during refinement), energy shift (ΔE_0), and the Debye Waller-factors (i.e. mean-square relative displacement, σ^2) were allowed to vary during the fitting process. The two paths used for Ni-N and Ni-Ni shells at R ca. 1.45 Å and R ca. 2.19 Å (not corrected for phase shift), respectively, were generated from the standards. Fittings were performed in all 3 k-weights to validate the model using an R-range between 1.0 - 3.0 Å (not shown). The k-space used for modelling was 3-14.5, 3-12.5, and 3-12.5 $Å^{-1}$ for Ni/NC, Ni/NC-D, and Ni/N-CNTs, respectively.

Preparation of the electrodes: The electrodes were prepared by drop-casting the ink of the catalysts on the carbon paper. The ink of the catalysts was made by sonicating the mixture the catalyst (5 mg), nafion (5wt%, 50 ul), and the isopropanol (1 ml). Then 40 ul of the ink was drop-casted on the two sides of the carbon paper (5 mm by 5mm) to make a catalyst loading of 0.4 mg cm^{-2}.

Electrochemical measurements: The electrochemical reduction of CO_2 was conducted in a batch-type cell with two chambers made from PTFE. The two chambers were separated by a Nafion membrane and each chamber contained 7 ml of 0.1 M $KHCO_3$ solution and 5 ml of headspace. CO_2 with a flow rate of 20 ml min^{-1} was dispersed into electrolyte through a fritted glass at the bottom of the cathodic chamber. Ag|AgCl (3 M KCl) electrode was used as the reference electrode. A platinum gauze was the counter electrode in the anodic chamber. The reaction was performed under constant current mode controlled by a galvanostat (Autolab PGSTAT302N). The value of the potential versus Ag/AgCl was converted to the scale of the reversible hydrogen electrode (RHE) using the equation: E (versus RHE) = E (versus Ag/AgCl (3 M KCl)) + 0.21 V + 0.059 * pH. The potential was post compensated by ohmic resistance that was determined by the current interrupt method.

The outlet of the CO_2 from cathodic chamber was connected to the gas chromatography (GC, SRI Instrument 8610C), which sampled the outlet gas every 7 minutes. The faradaic efficiency (FE) was calculated using FE = $\frac{nFC_ivP}{jRT}$, in which n is the number of transferred electron to produce one molecule of the target product i, F is the faradaic efficiency, C_i is the concentration of the target product i determined by GC, v is the flow rate of CO_2 of the inlet, P and T are the pressure (101325 Pa) and temperature (22 °C) of the gas sampled by the GC sample loop, respectively, j is the total current when sampling, R is the gas constant.

Supporting Figures and Tables

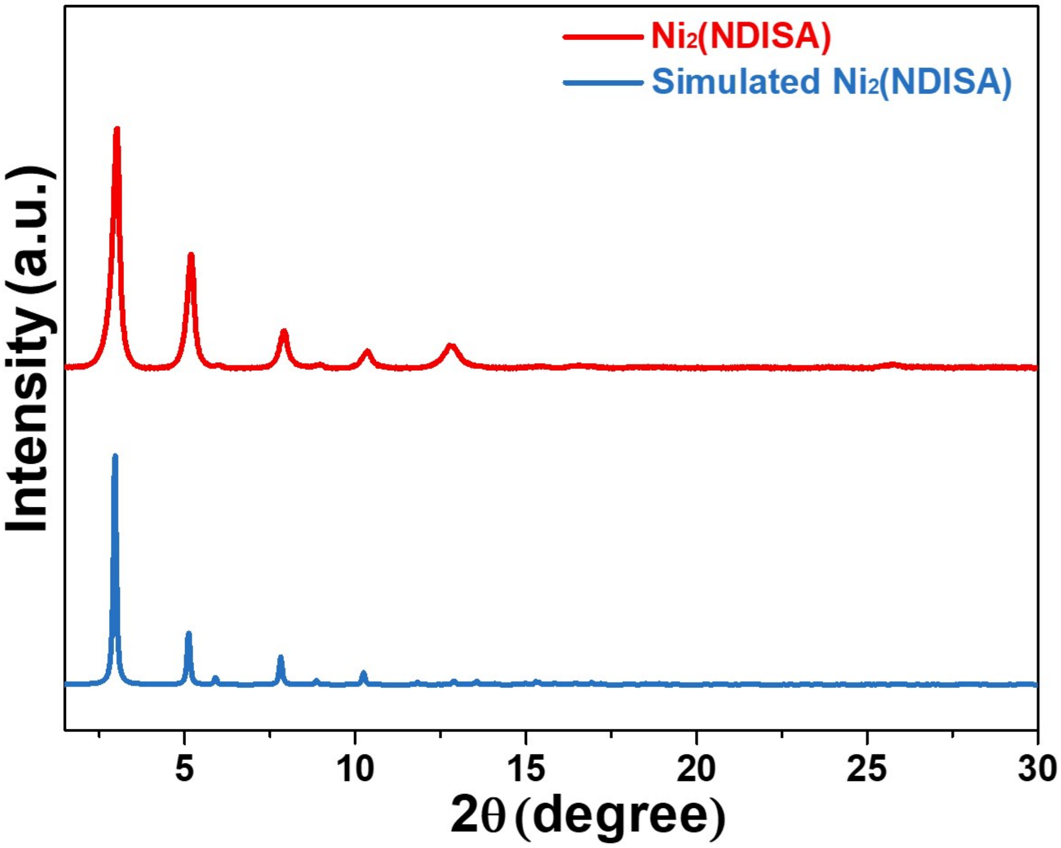

Fig. S1 XRD patterns of the synthesized Ni_2(NDISA) and the simulated pattern.

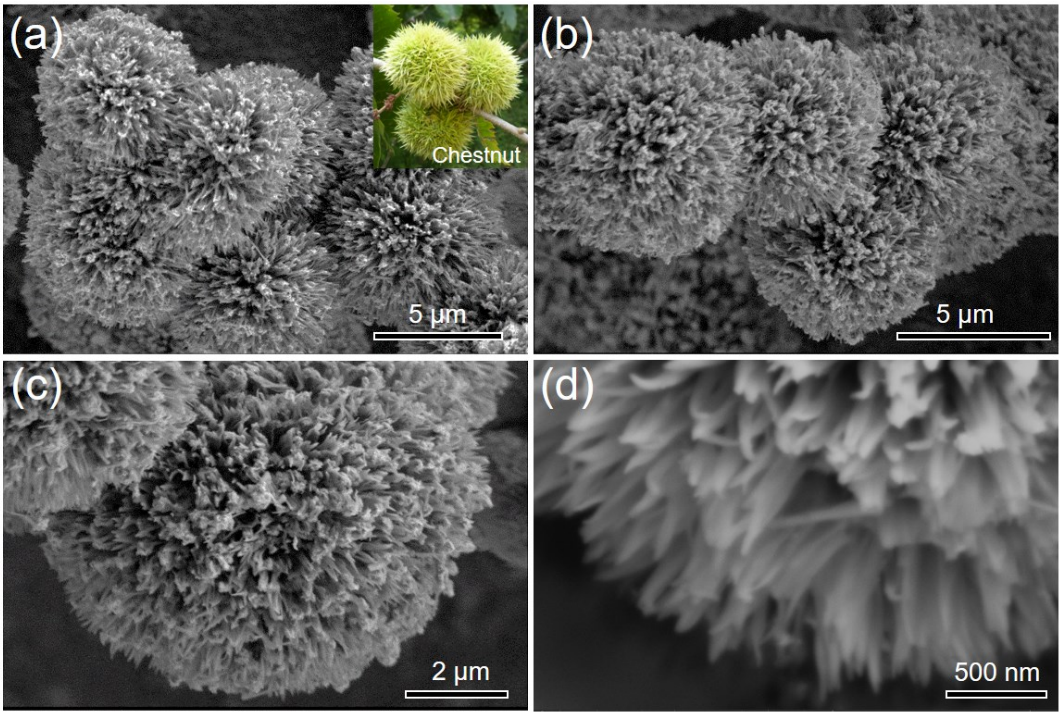

Fig. S2 SEM images of the synthesized Ni_2(NDISA) MOF.

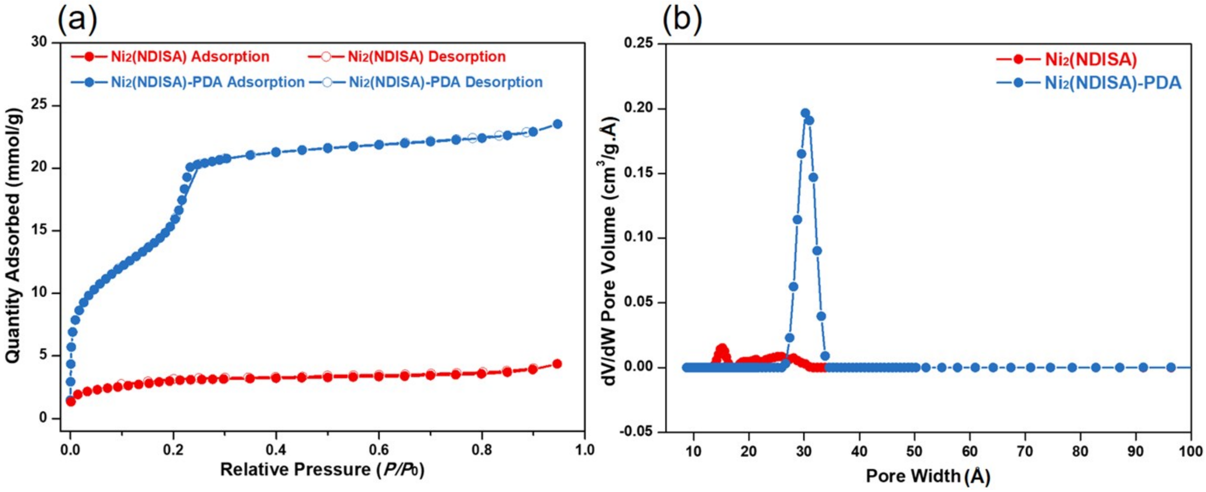

Fig. S3 N_2 adsorption isotherms (a) and the corresponding pore size distribution (b) of the synthesized Ni_2(NDISA) MOF (red) and the Ni_2(NDISA)-PDA composites (navy).

.

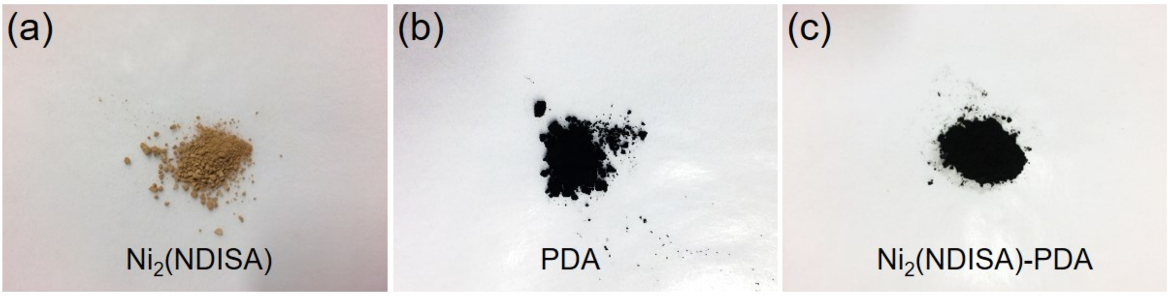

Fig. S4 Digital photos of the synthesized Ni_2(NDISA) (a), polydopamine polymer (b) and Ni_2(NDISA)-PDA composite (c).

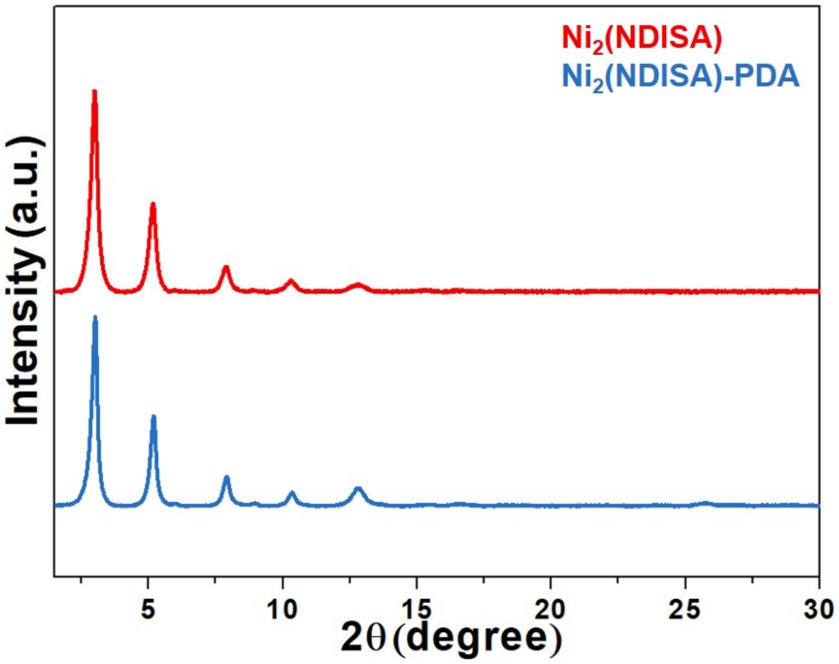

Fig. S5 XRD patterns of the synthesized Ni_2(NDISA) and the Ni_2(NDISA)-PDA composite.

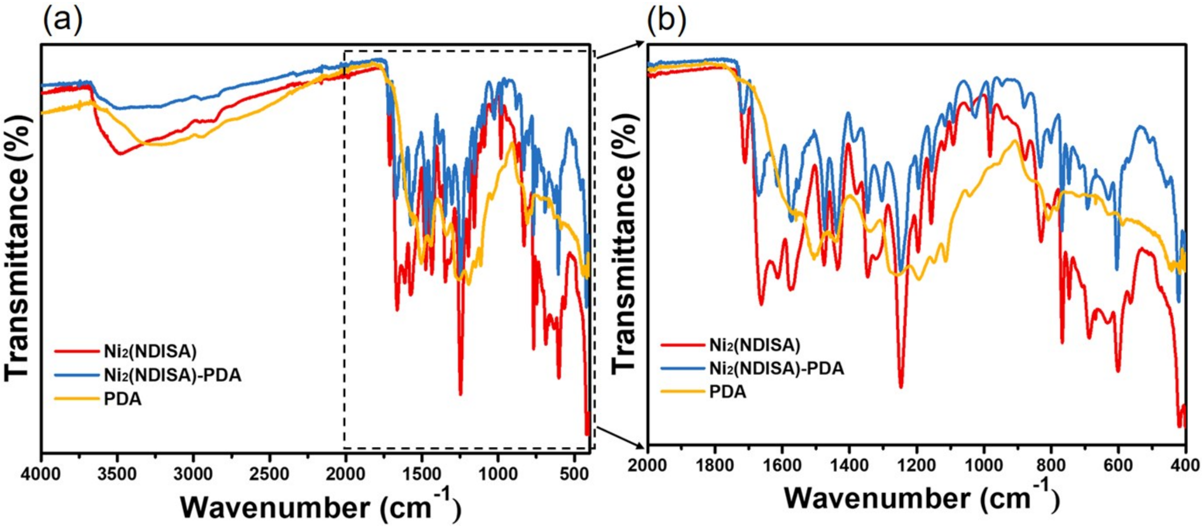

Fig. S6 FT-IR spectrum of the Ni_2(NDISA), Ni_2(NDISA)-PDA and PDA. Because of the similar functional groups in Ni_2(NDISA) and PDA, the FT-IR could not distinguish the presence of PDA very well.

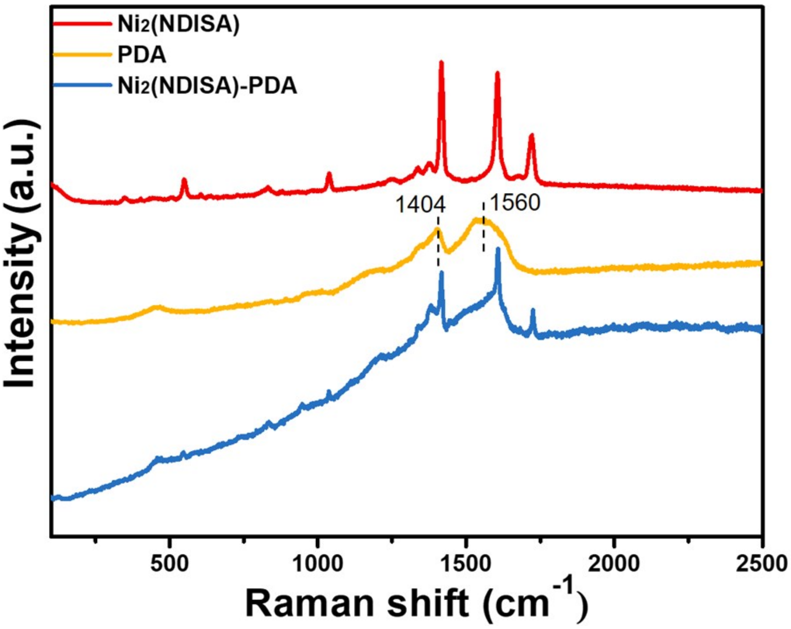

Fig. S7 Raman spectrum of the Ni_2(NDISA), Ni_2(NDISA)-PDA and PDA. The peaks at 1404 and 1560 cm^{-1} correspond to the stretching and deformation of aromatic rings of the catechols after polymerization of free-base dopamine, respectively.[7, 8] The broad width of the peaks should ascribe to the complicated environment of the PDA structure.

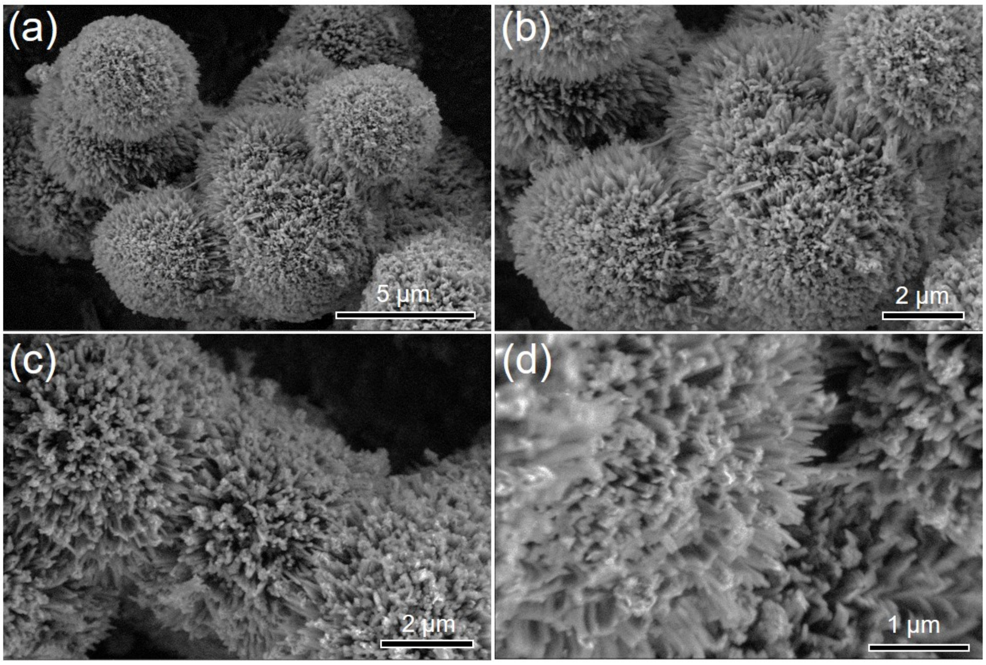

Fig. S8 SEM images of the synthesized Ni_2(NDISA)-PDA composite.

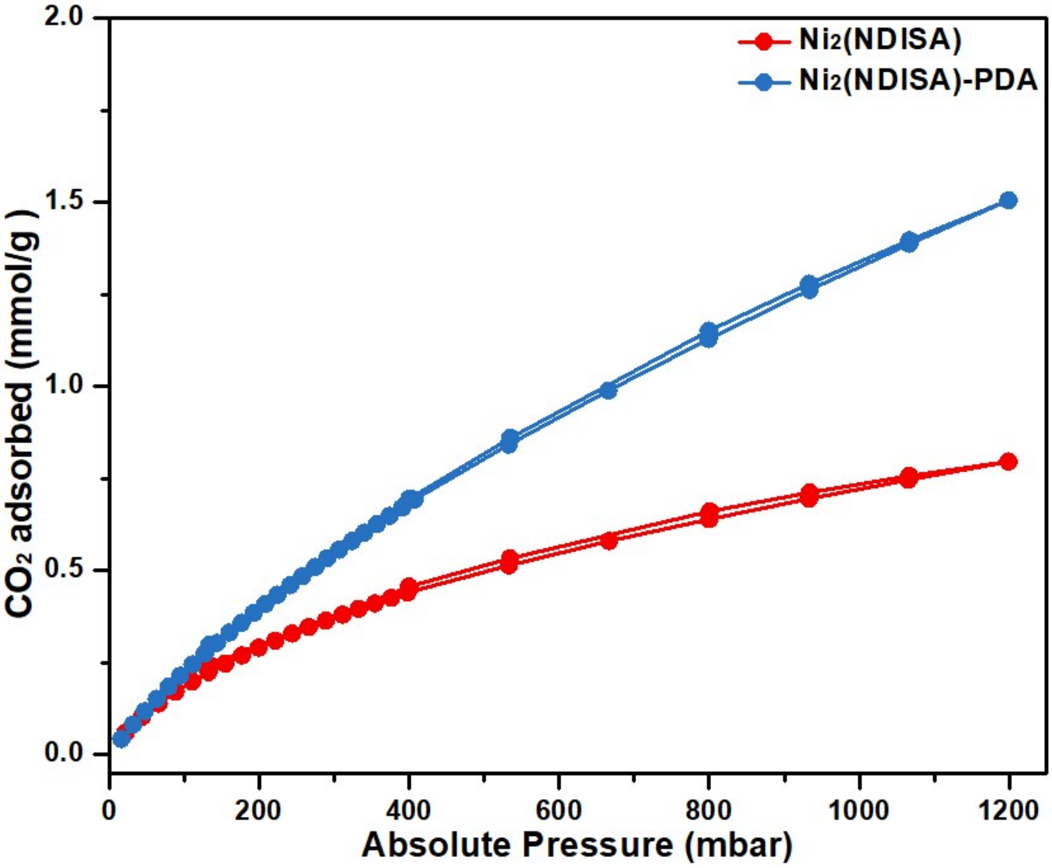

Fig. S9 CO_2 adsorption isotherm of Ni_2(NDISA) (orange) and Ni_2(NDISA)-PDA (red) at 298 K.

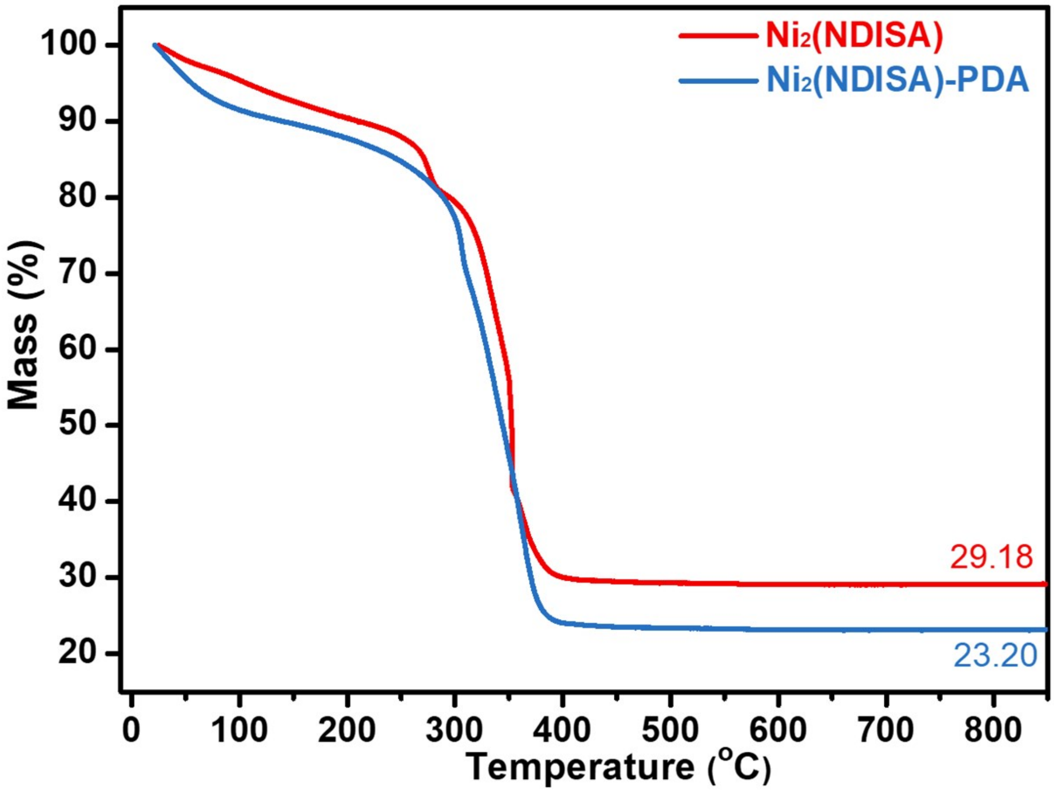

Fig. S10 Thermogravimetric analysis of Ni_2(NDISA) and Ni_2(NDISA)-PDA composite revealed the polymer loading in Ni_2(NDISA)-PDA was 20.5 wt%: (1-23.20/29.18)*100% = 20.5 wt%. The TGA analysis was tested in the air atmosphere with the ramping rate of 5 ^{o}C/min to 850 ^{o}C.

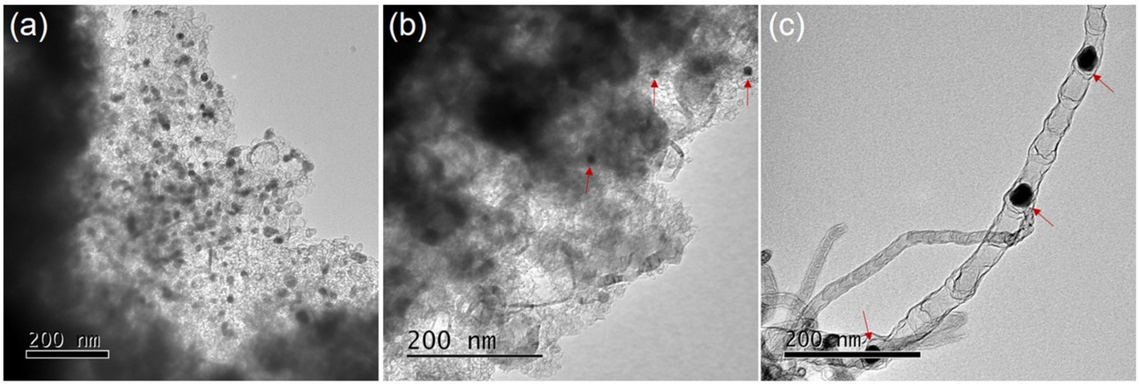

Fig. S11 Bright-field TEM images of the Ni/NC (a), Ni/NC-D (b) and Ni/N-CNTs sample. Remaining Ni NPs are marked by red arrows in (b) and (c). The Ni NPs size in Ni/NC (a), Ni/NC-D (b) and Ni/N-CNTs is about 19, 15, 31 nm, respectively.

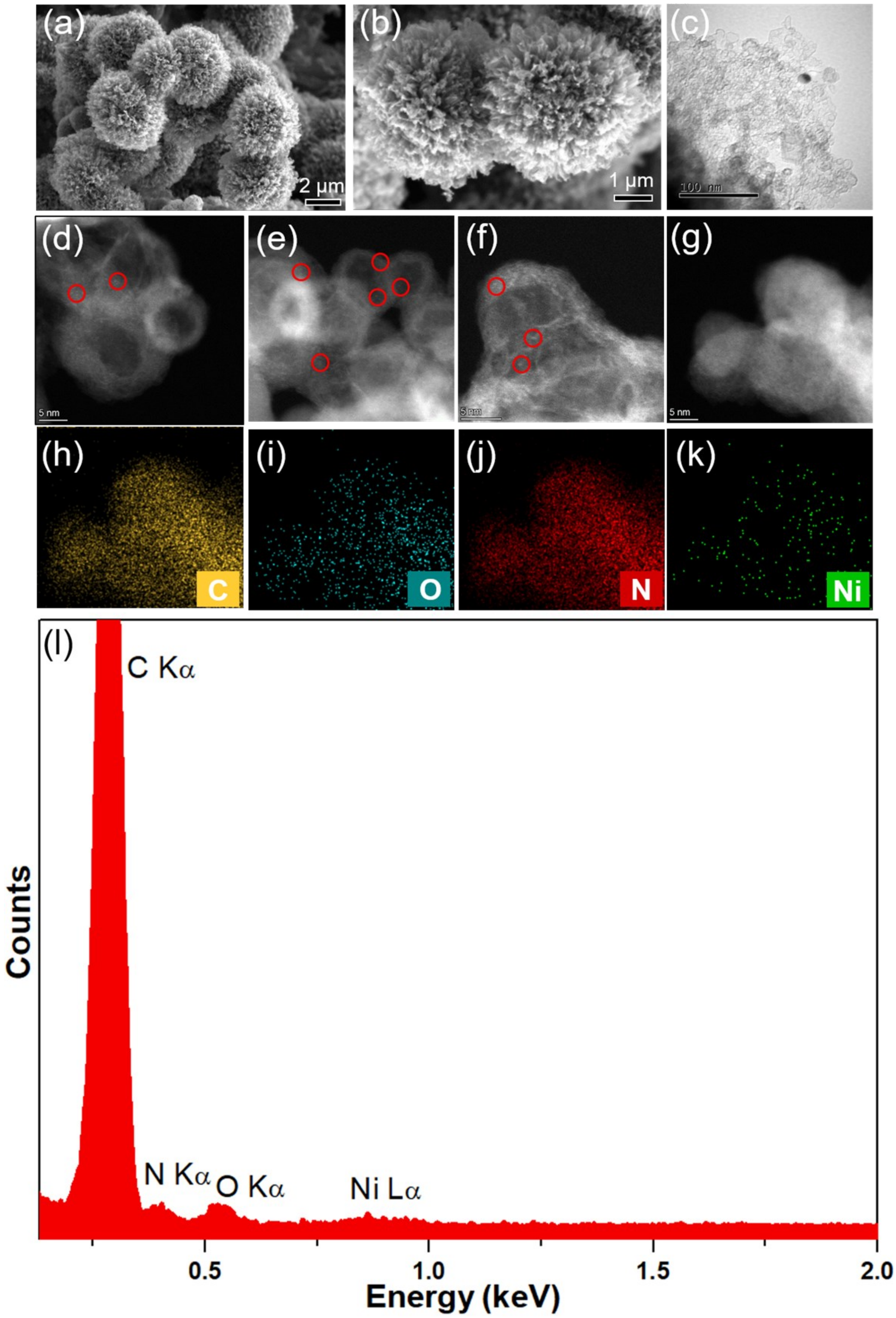

Fig. S12 SEM (a,b), bright-field TEM (c) and HAADF-STEM (d-g) images of Ni/NC sample. (h-k) are the STEM-EDXS elemental maps of C, O, N and Ni in the Ni/NC sample shown in (g). Images (c-f) show hollow carbon structures present in the Ni/NC samples, which are from the gas releasing during the calcination step and the Ni NPs positions before the acid-etching.

Single-atom nickel sites can be observed clearly in HAADF-STEM images (d-f). Part metal single atoms are indicated by red circles in images (d-f).

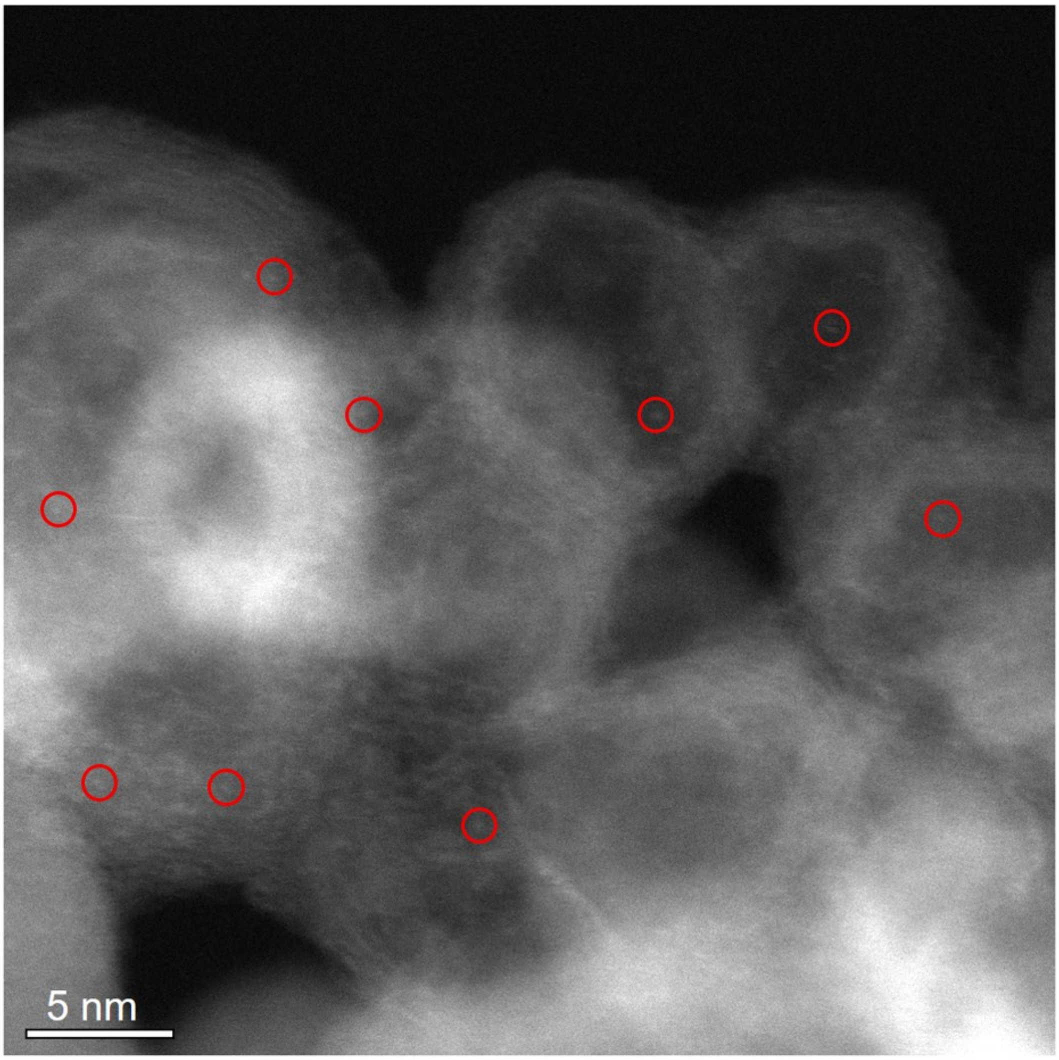

Fig. S13 HAADF-STEM image of Ni/NC sample. Single-atom nickel sites can be observed clearly and part of them is indicated by red cycles.

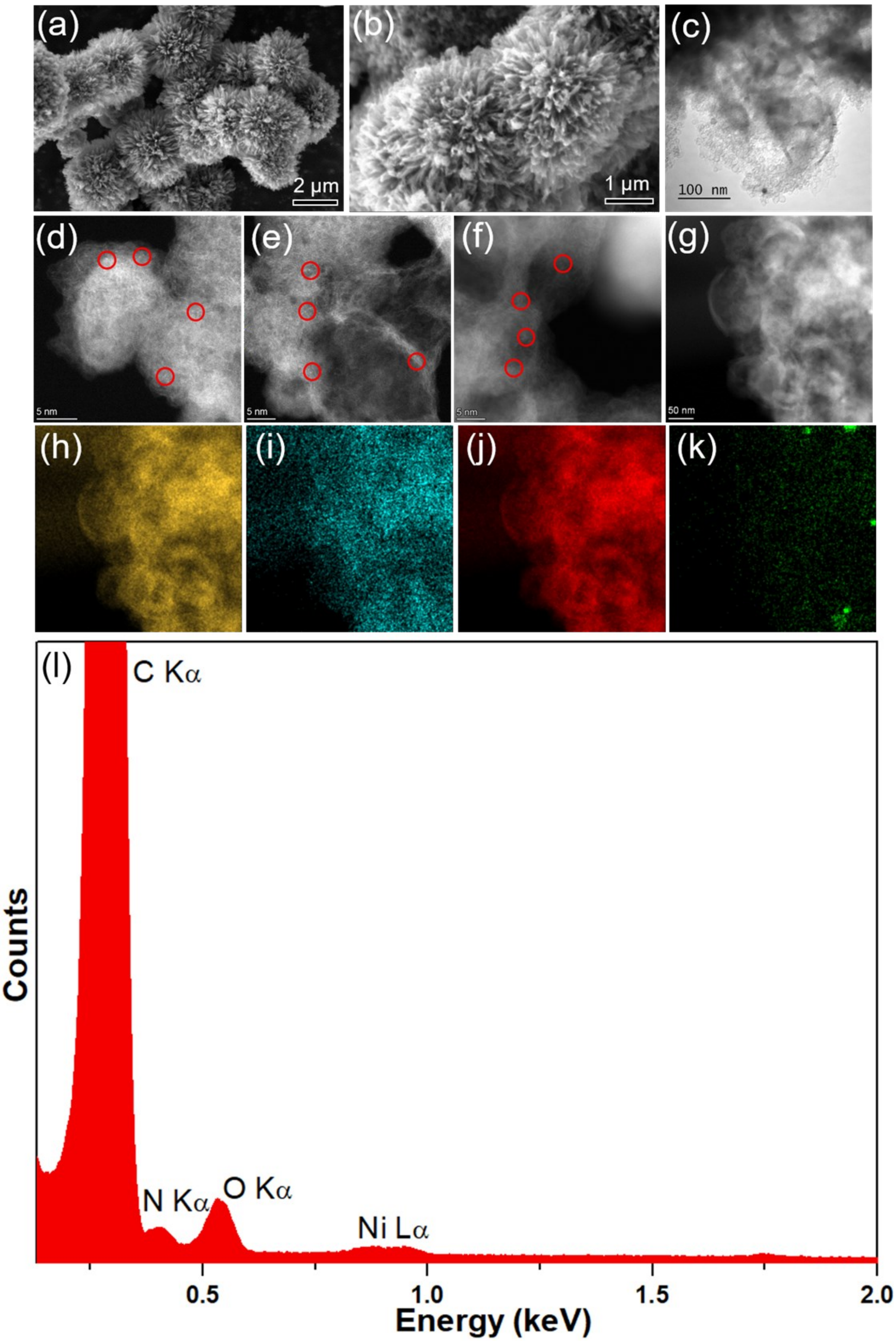

Fig. S14 SEM (a,b), bright-field TEM (c) and HAADF-STEM (d-g) images of Ni/NC-D sample. (h-k) are the STEM-EDXS elemental maps of C, O, N and Ni in the Ni/NC-D sample shown in (g). Images (c), (e) and (g) show hollow carbon structures present in the Ni/NC-D samples, which are from the gas releasing during the calcination step and the Ni NPs positions before the acid-etching. Single-atom nickel sites can be observed clearly in HAADF-STEM images (d-f). Part metal single atoms are indicated by red circles in images (d-f).

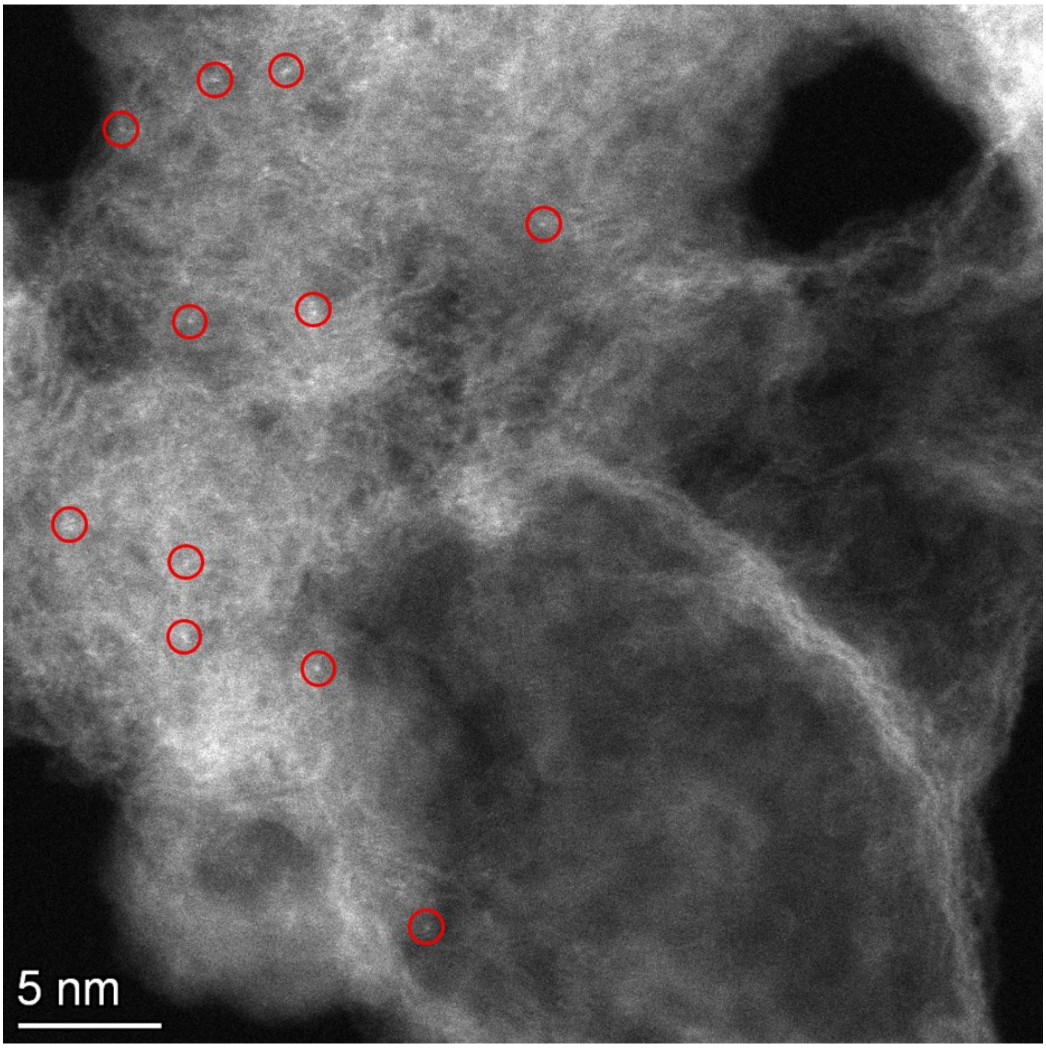

Fig. S15 HAADF-STEM image of Ni/NC-D sample. Single-atom nickel sites can be observed clearly and part of them is indicated by red cycles.

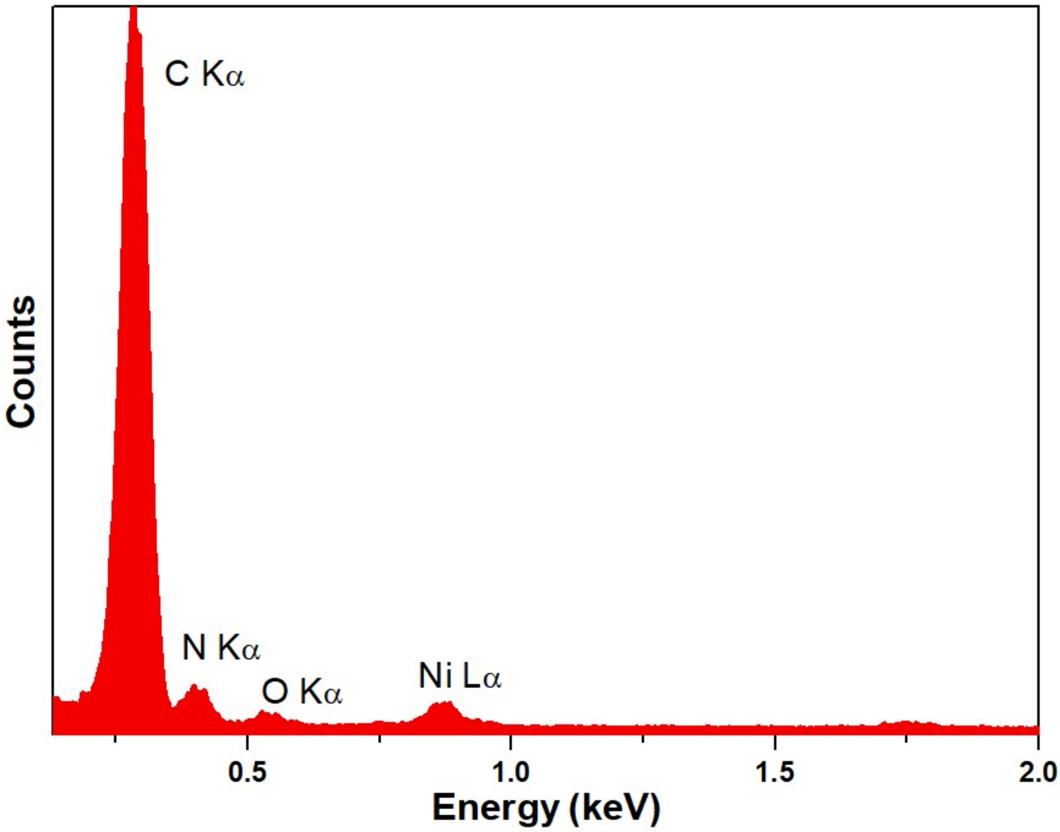

Fig. S16 STEM-EDX spectrum of the Ni/N-CNTs sample.

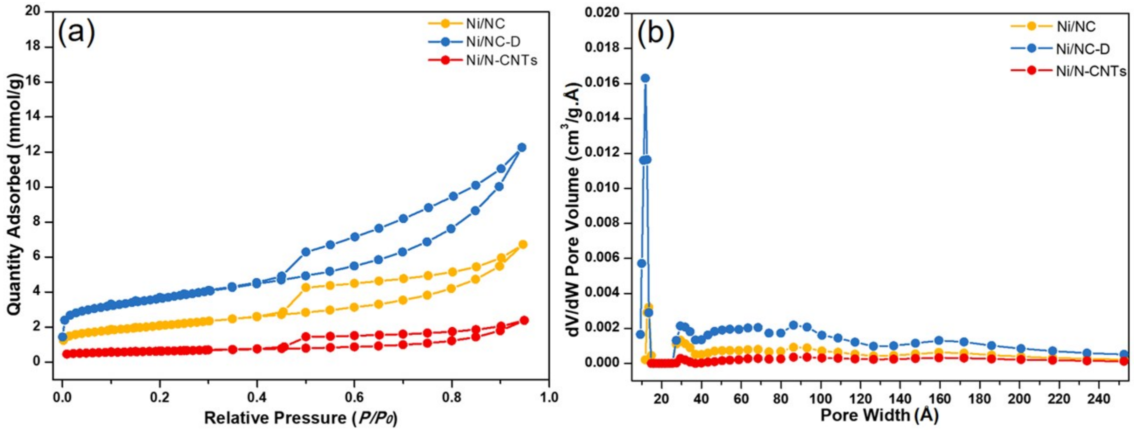

Fig. S17 N_2 adsorption isotherms (a) and the corresponding pore size distribution (b) of Ni/NC, Ni/NC-D and Ni/N-CNTs.

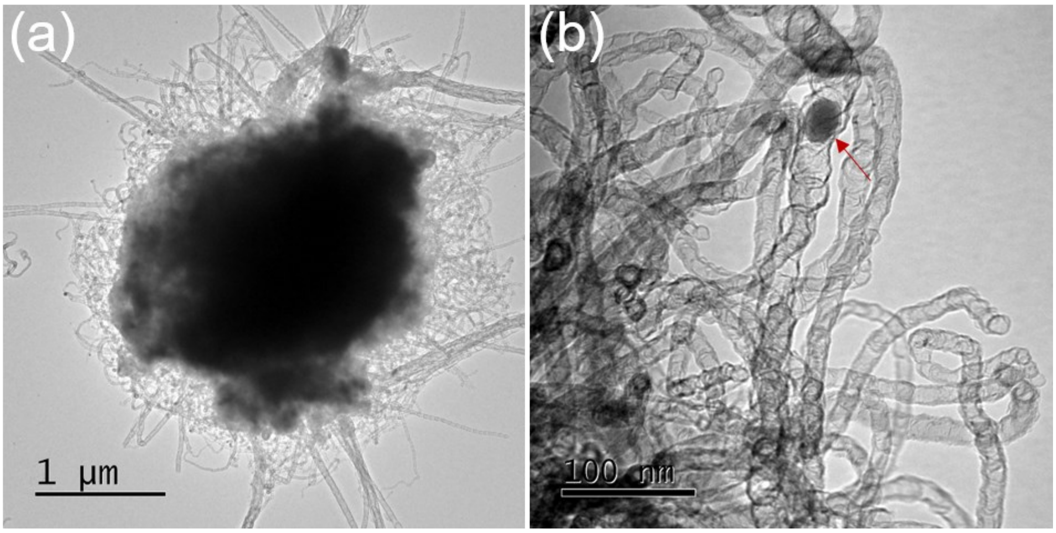

Fig. S18 Bright-field TEM images of the Ni/N-CNTs sample. Remaining Ni NP is marked by red arrows.

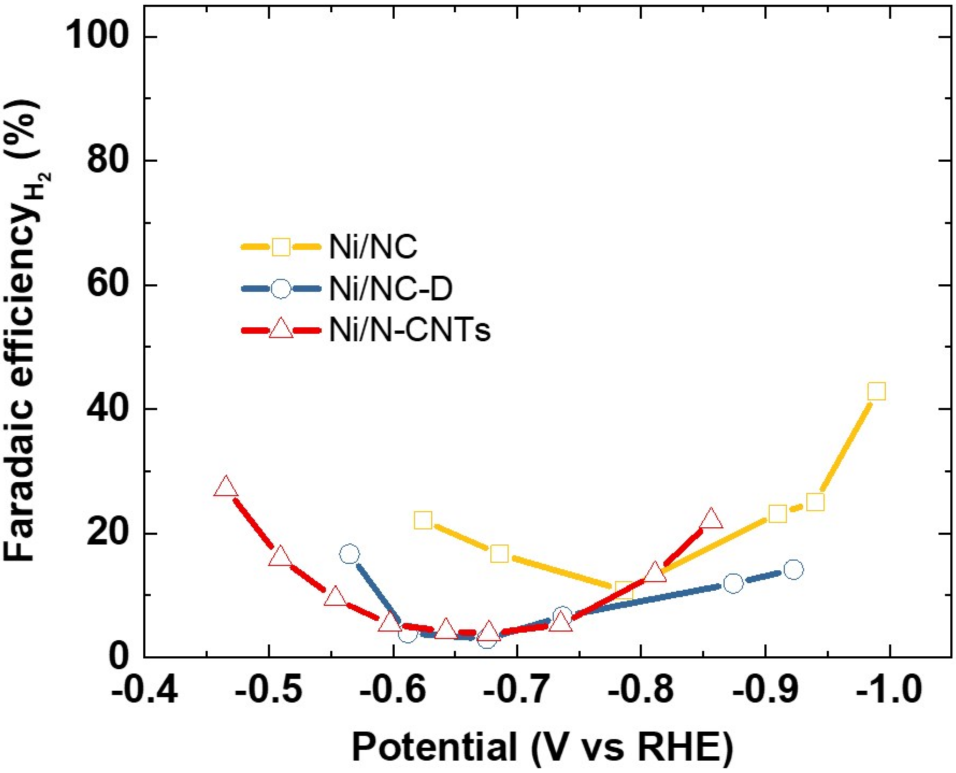

Fig. S19 Faradaic efficiency for H_2 of Ni/NC, Ni/NC-D and Ni/N-CNTs catalysts.

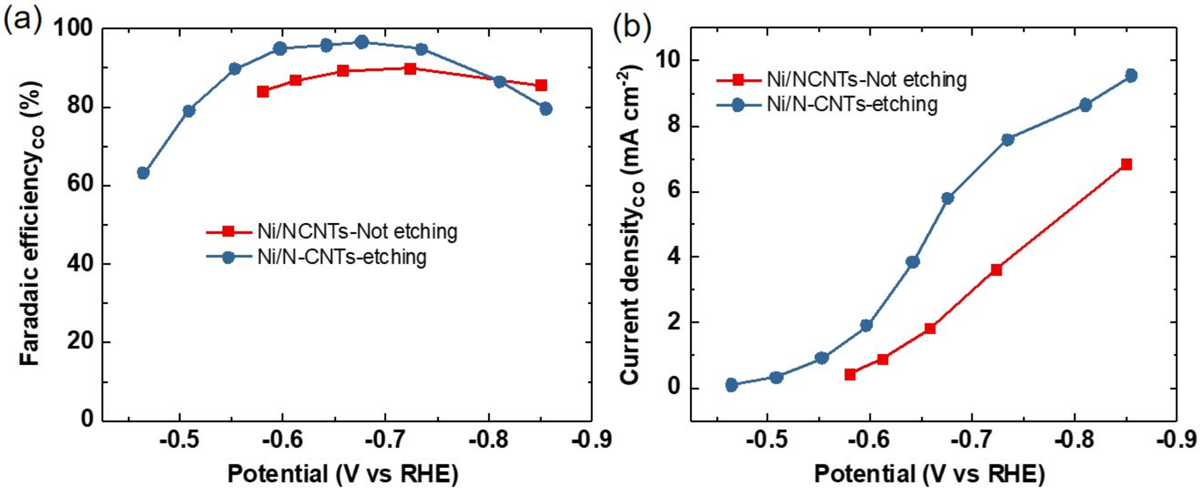

Fig. S20 CO faradaic efficiency (a) and CO partial current density of the Ni/N-CNTs sample with and without acid etching.

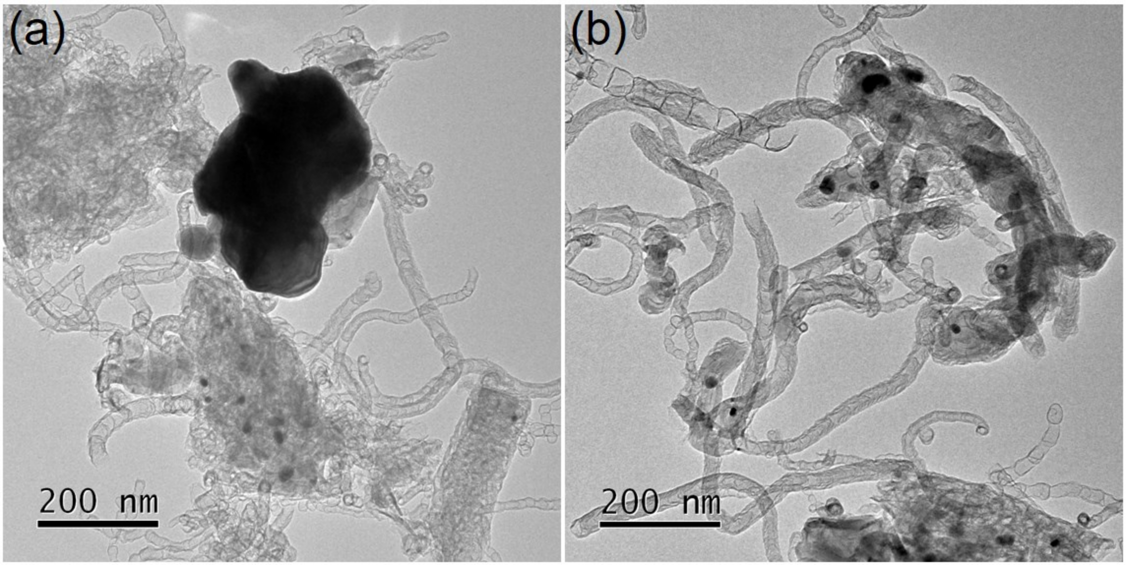

Fig. S21 Bright-field TEM images of the Ni/N-CNTs sample without acid etching. Agglomerated Ni particles can be observed on the surface of CNTs (a) and inside of CNTs (b).

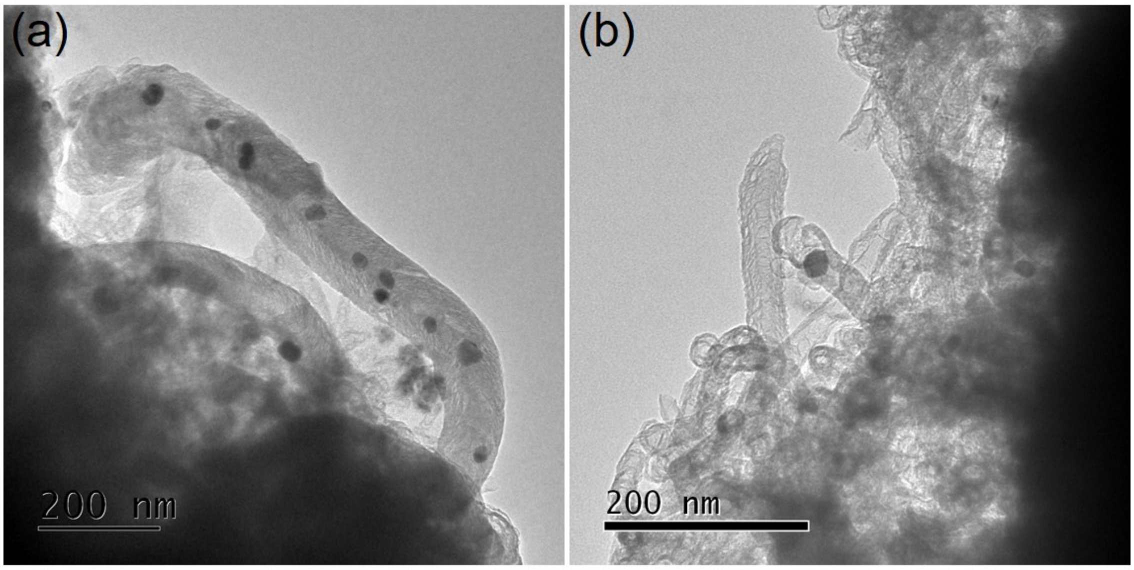

Fig. S22 Bright-field TEM images of the Ni/N-CNTs sample after 1 h of CO_2 electroreduction at 4 mA cm^{-2}.

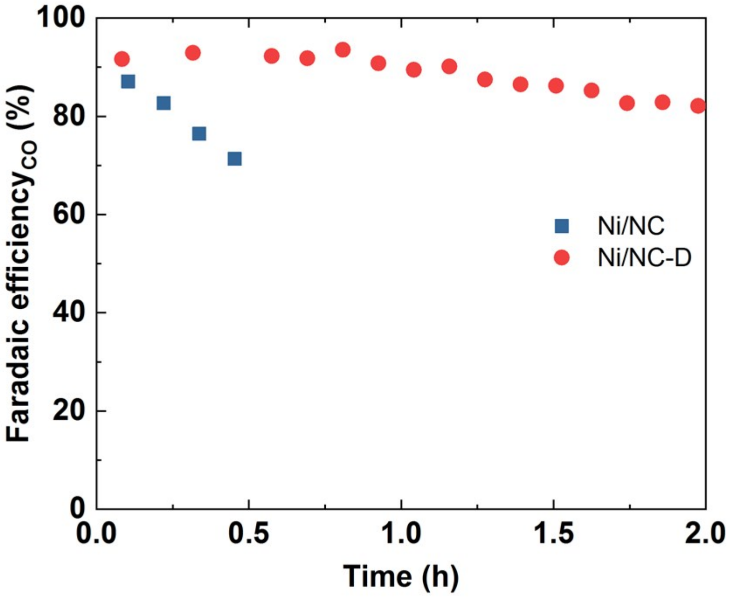

Fig. S23 CO Faradaic efficiency of Ni/NC and Ni/NC-D as a function of reaction time. Ni/NC was evaluated at constant 2 mA cm^{-2}, and Ni/NC-D was evaluated at constant 4 mA cm^{-2}. The electrolyte is 0.1 M $KHCO_3$ saturated by CO_2.

Table S1. Content of Ni and different N species in our catalysts extracted from XPS data. Total metal and nitrogen content are calculated from measured XP spectra areas corrected using atomic sensitivity factors.

Sample	Ni atom %	Nitrogen atom %	Fitting of nitrogen moieties / atom%				
			Ni-N_x	Pyridinic N	Pyrrolic N	Graphic N	N-O_x
Ni/NC	0.2	1.3	9.0	19.5	48.1	14.1	9.3
Ni/NC-D	0.1	1.2	7.0	16.8	51.6	16.0	8.5
Ni/N-CNTs	0.9	6.2	18.3	36.7	29.5	9.2	6.4

It should be noted that although Ni/NC show slightly higher Ni-N_x ratio than that for Ni/NC-D, the surface area of Ni/NC-D is about 1.8 times higher than Ni/NC, thus with the same mass loading of catalyst (0.4 mg/cm^2), the overall Ni-N_x for Ni/NC-D is higher than Ni/NC.

Table S2. EXAFS details. Summary of the optimized parameters from the EXAFS fitting of the three samples i.e. Ni/NC, Ni/NC-D, and Ni-N-CNTs. The fits were performed on a ΔR = 1-3 Å, and the k-space used was equal to 3-14.5, 3-12.5, and 3-12.5 Å^{-1} for Ni/NC, Ni/NC-D, and Ni/N-CNTs, respectively. Coordination number (C.N.), interatomic distances ($R_{final} = R_0 + \Delta R$), energy shift ($\Delta E_0$), Debye Waller-factors (σ^2), and R-factor (the goodness of fit parameter) are shown.

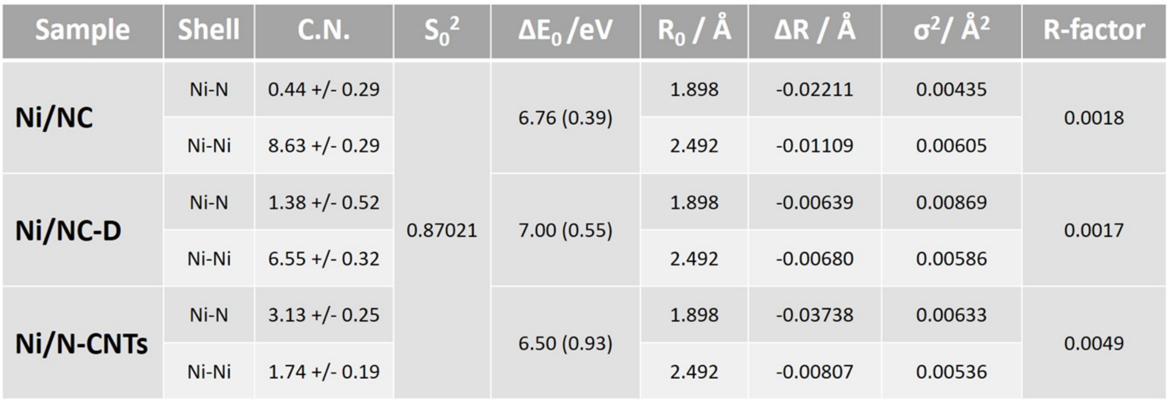

Sample	Shell	C.N.	S_0^2	ΔE_0 /eV	R_0 / Å	ΔR / Å	σ^2/ Å^2	R-factor
Ni/NC	Ni-N	0.44 +/- 0.29	0.87021	6.76 (0.39)	1.898	-0.02211	0.00435	0.0018
	Ni-Ni	8.63 +/- 0.29			2.492	-0.01109	0.00605	
Ni/NC-D	Ni-N	1.38 +/- 0.52		7.00 (0.55)	1.898	-0.00639	0.00869	0.0017
	Ni-Ni	6.55 +/- 0.32			2.492	-0.00680	0.00586	
Ni/N-CNTs	Ni-N	3.13 +/- 0.25		6.50 (0.93)	1.898	-0.03738	0.00633	0.0049
	Ni-Ni	1.74 +/- 0.19			2.492	-0.00807	0.00536	

References:

1. D. T. Sun, L. Peng, W. S. Reeder, S. M. Moosavi, D. Tiana, D. K. Britt, E. Oveisi and W. L. Queen, *ACS Cent. Sci.*, 2018, **4**, 349-356.
2. L. Peng, S. Yang, S. Jawahery, S. M. Moosavi, A. J. Huckaba, M. Asgari, E. Oveisi, M. K. Nazeeruddin, B. Smit and W. L. Queen, *J. Am. Chem. Soc.*, 2019, **141**, 12397-12405.
3. K. AlKaabi, Casey R. Wade and M. Dincă, *Chem*, 2016, **1**, 264-272.
4. O. Muller, M. Nachtegaal, J. Just, D. Lutzenkirchen-Hecht and R. Frahm, *J. Synchrotron Radiat.*, 2016, **23**, 260-266.
5. A. H. Clark, J. Imbao, R. Frahm and M. Nachtegaal, *J. Synchrotron Radiat.*, 2020, **27**, 551-557.
6. B. Ravel and M. Newville, *J. Synchrotron Radiat.*, 2005, **12**, 537-541.
7. B. Fei, B. Qian, Z. Yang, R. Wang, W. C. Liu, C. L. Mak and J. H. Xin, *Carbon*, 2008, **46**, 1795-1797.
8. J. Ryu, S. H. Ku, H. Lee and C. B. Park, *Adv. Funct. Mater.*, 2010, **20**, 2132-2139.